

Magnetic shielding properties of a superconducting hollow cylinder containing slits: modelling and experiment

J-F Fagnard¹, S Elschner², A Hobl³, J Bock³, B Vanderheyden¹ and P Vanderbemden¹

(1) SUPRATECS and Department of Electrical Engineering and Computer Science B28, Sart-Tilman, B-4000 Liège, Belgium

(2) University of Applied Science Mannheim, D-68163 Mannheim, Germany

(3) Nexans SuperConductors GmbH, D-50531 Hürth, Germany

E-mail : Philippe.Vanderbemden@ulg.ac.be

Abstract. This paper deals with the magnetic properties of bulk high temperature superconducting cylinders used as magnetic shields. We investigate, both numerically and experimentally, the magnetic properties of a hollow cylinder with two axial slits which cut the cylinder in equal halves. Finite Element Method (FEM) modelling has been used with a three-dimensional geometry to help us in understanding how the superconducting currents flow in such a cut cylinder and therefore how the magnetic shielding properties are affected, depending on the magnetic field orientation. Modelling results show that the slits block the shielding currents flow and act as an “entrance channel” for the magnetic flux lines. The contribution of the slits to the total flux density that enters the cylinder is studied through the angle formed between the applied field and the internal field. The modelled data agree nicely with magnetic shielding properties measured on a bulk Bi-2212 hollow cylinder at 77 K. The results demonstrate that the magnetic flux penetration in such a geometry can be modelled successfully using only two parameters of the superconductor (constant J_c and n value), which were determined from magnetic measurements on the plain cylinder.

PACS codes : 74.25.-q, 74.25.Sv, 74.72.-h, 41.20.Gz

1. Introduction

An enclosure made of superconducting material can be regarded as an excellent passive screen against magnetic fields over a large frequency range [1-3]. At low frequency in particular, the efficiency of superconductors is usually higher than that of conventional ferromagnets [1, 2]. A low magnetic field background is encountered in various domains, including SQUIDS (superconducting quantum interference devices) [4], magneto-encephalography [5], cryogenic current comparators [6] or naval military applications [7]. The present work deals with enclosures made of bulk high temperature superconductors (HTS). They can be used either at liquid nitrogen temperature (77 K) – at which magnetic shielding occurs up to a few tens of mT – or at low temperature (10 K and below) where shielding of magnetic fields in excess of 1 tesla was demonstrated recently [8, 9]. Several materials are candidates for efficient magnetic screens, including MgB_2 [8, 10], $YBa_2Cu_3O_7$ [3, 11] or Bi-based compounds [12-15]. The basic shape for studying magnetic shielding is a hollow cylinder of typically of 2-5 cm diameter and 5-20 cm height. In view of increasing the size of the shielded volume, either cylinders of larger size should be synthesized, or the cylinder could be cut in two halves subsequently separated in order to make a larger structure, as illustrated in figure 1(a). In the present work we model and characterize the magnetic shielding properties of a bulk hollow superconductor with two axial slits (framed illustration in figure 1(a)). The aim is to investigate whether numerical modelling is able to predict and quantify the effect of such slits on the magnetic shielding performances. The modelled data will be compared to experiment carried out on bulk $Bi_2Sr_2CaCu_2O_8$ (Bi-2212) materials obtained by melt cast process (MCP) [16-18].

The magnetic properties of superconducting hollow cylinders have been documented extensively in the literature [19-21]. The advantage of a passive shield (i.e., a simple superconducting cavity) over an active shield (i.e., a set of coils fed with appropriate currents) is that it does not require an *a priori* knowledge of the orientation of the magnetic field to be screened. Basically, two simple configurations can be considered for a cylinder : (i) the *axial* configuration, i.e., the external magnetic field is parallel to the axis of the tube, and (ii) the *transverse* configuration, i.e., the external magnetic field is perpendicular to the axis of the tube. The *axial* configuration is the simplest to consider. When the aspect ratio (height / diameter) of the cylinder is large enough (let say > 3), valuable information can be obtained from a one-dimensional analysis (1D) based on the Bean model [22, 23], possibly with a field-dependent critical current density J_c [21, 24]. For short cylinders, finite size effects need to be considered and a 2D model should be used in order to account for the two mechanisms of field penetration, i.e. from the lateral surface and through the opening ends [14, 25, 26]. The investigation of magnetic screening in the *transverse* configuration involves at least a 2D model. At low applied

field (i.e., before the magnetic induction reaches the inner wall of the cylinder), the magnetic flux penetration profiles are similar to those in a bulk cylindrical wire subjected to a transverse field [27] and exhibit an “eye-shape” structure. The flux profiles of an infinite cylinder in transverse fields can be obtained semi-analytically [28-30], using a semi-analytical model developed by Brandt [31, 32] or a finite-element model [33]. In the present work dealing with a hollow cylinder containing two axial slits, only the transverse configuration will be studied, as illustrated in figure 1(b). We will take advantage of the possibilities offered by 3D finite element modelling [34-37] to investigate the flux penetration by taking into account both the finite height effects and the magnetic flux density through the slit.

Our paper is organized as follows. In Section 2, we present the finite element model and the constitutive laws that are used. Section 3 describes the experimental system used to achieve precise magnetic shielding measurements. The modelling results are presented and analyzed in Section 4. These results will be compared to experimental data obtained with the same conditions. The conclusions are drawn in Section 5.

2. Model

The numerical modelling results are obtained by using the *Finite Element Method* (FEM), using the \mathbf{A} - ϕ formulation [34]. The Maxwell equations are solved for two independent variables: (i) the vector potential, \mathbf{A} , and (ii) the scalar potential, ϕ , defined as:

$$\mathbf{B} = \mathbf{B}_{\text{self}} + B_{\text{app}}(t)\mathbf{e}_z = \nabla \times \mathbf{A}_{\text{self}} + \nabla \times \mathbf{A}_{\text{app}}, \quad (1)$$

$$\mathbf{E} = -\frac{\partial \mathbf{A}_{\text{self}}}{\partial t} - \frac{\partial \mathbf{A}_{\text{app}}}{\partial t} - \nabla \phi. \quad (2)$$

where \mathbf{B}_{self} is the magnetic flux density induced by the HTS, $\mathbf{B}_{\text{app}}(t)$ is the uniform applied magnetic flux density; \mathbf{A}_{self} and \mathbf{A}_{app} are the corresponding vector potentials. These fields are approximated by edge functions (1st order):

$$\mathbf{A} = \sum_{i=1}^M a_i \mathbf{A}_i \quad (3)$$

that ensure the continuity of the tangential component of \mathbf{A} and node functions (1st order):

$$\phi = \sum_{j=1}^N b_j \phi_j, \quad (4)$$

that ensure the continuity of ϕ .

The superconducting properties are modelled using an E - J power law, i.e.

$$E(J) = E_c \left(\frac{J}{J_c} \right)^n \quad (5)$$

where the two material-related parameters, the critical exponent n and the critical current density J_c , are determined from magnetic measurements on a plain cylinder, as detailed in the next section. In order to limit the number of modelling parameters and simplify the interpretation of results, both n and J_c are assumed to be field-independent.

Using the above formulation, Maxwell equations are reduced to the coupled equations:

$$\nabla \times \nabla \times \mathbf{A} = \mu_0 \sigma(\mathbf{A}, \phi) \left(-\frac{\partial \mathbf{A}_{self}}{\partial t} - \frac{\partial \mathbf{A}_{app}}{\partial t} - \nabla \phi \right) \quad (6)$$

$$\nabla \cdot \left\{ \sigma(\mathbf{A}, \phi) \left(-\frac{\partial \mathbf{A}_{self}}{\partial t} - \frac{\partial \mathbf{A}_{app}}{\partial t} - \nabla \phi \right) \right\} = 0 \quad (7)$$

where σ is the power-law conductivity:

$$\sigma(\mathbf{E}) = \frac{J_c}{E_c^{1/n}} (|\mathbf{E}|)^{1-n}. \quad (8)$$

The equations have to be solved with the boundary (Dirichlet) conditions at infinity:

$$\mathbf{A} = 0, \quad (9)$$

and

$$\phi = 0, \quad (10)$$

that have been implemented by using a Jacobian transformation for sending the outer surface of a spherical shell to infinity [38].

The solver used for the modelling is the open-source solver GetDP developed by the Applied and Computational Electromagnetics research unit of the University of Liège [39]. Its description and details of the code used for superconducting material modelling were described earlier [34, 39, 40].

The geometry studied in the present work is a hollow cylinder of finite height with two slits made in a vertical plane along a diameter. Because of the presence of the slits, the structure is not axisymmetric and 2D simulations cannot take account of the effect of a transverse magnetic field applied at arbitrary angle; for this reason 3D modelling will be used. Because of the limited number of nodes available to allow a full 3D calculation in a decent time, however, modelling will be carried out on a shorter

sample with height L ($= 20$ mm) being comparable to the average diameter D ($= 17.5$ mm), as illustrated schematically in the right-hand part of figure 1(b). The thickness of the cylinder wall is 5.5 mm and the two halves are separated from each other by a 1 mm gap. This gap size was chosen to properly mesh the regions inside the slits. The resulting modelled and meshed structure involves 45,000 nodes in volume and 250,000 tetrahedra. Due to the restriction to the sample height for modelling, the experiments are carried out on both long (80 mm) and short (20 mm) samples (see next section).

The use of a 3D model requires some caution. In many problems with a specific symmetry, the current density vectors are forced to be everywhere perpendicular to the local magnetic flux density. In this case, the constitutive equations are well established and the results obtained with the finite element method are trustworthy. In the opposite situation of a system with no particular symmetry, as is the case for the geometry investigated here, current densities may locally develop components which are parallel to the magnetic flux density (longitudinal currents). Hence classical constitutive equations may no longer be valid and unusual critical states should be considered [41]. This largely debated problem [42, 43] is not directly addressed in the present work. Care should thus be taken in interpreting the results obtained by 3D modelling, as the contribution of longitudinal currents in the magnetic phenomena arising in bulk superconductors is still not assessed. Besides these limitations, the modelling is expected to give relevant information about the penetration of the magnetic field inside the superconductor, the flow of the persistent currents and the way they are affected by the presence of the slits which break the symmetry of the system.

3. Experiment

The studied sample is a hollow cylinder of $\text{Bi}_2\text{Sr}_2\text{CaCu}_2\text{O}_8$ (Bi-2212) produced by the melt casting process [16]. This cylinder is then cut axially into equal halves using a wire saw. The two halves are insulated with Kapton tape, resulting in a gap width of ≈ 200 μm . The dimensions of the sample are presented in Table 1. The experiments are first carried out on a long sample (80 mm length), then this sample is cut in two unequal parts (20 mm and 60 mm) and the same data are recorded on the shorter sample which has the same length as the modelled sample (20 mm). Magnetic shielding measurements are carried out using a home made set up designed for the characterization of relatively large hollow cylinders (up to 80 mm length) in both axial and transverse geometries. The applied magnetic field is generated by a long copper coil (length 45 cm, diameter 20 cm) fed by a HP6030A DC power supply. The applied magnetic field at the centre of the coil can reach $\mu_0 H_{\text{app}} = 36$ mT. The field can be ramped at a constant sweep rate between 5 $\mu\text{T/s}$ and 20 mT/s. In the present work, a fixed sweep rate of 1

mT/s is always used. The magnetic flux density at the centre of the cylinder is measured with a high sensitivity Hall probe (Arepoc - HHP-MP), recorded by a PCI-6281 National Instrument Data Acquisition Card controlled by a PC running Labview®. All measurements are carried out in liquid nitrogen (77 K). Two concentric mu-metal ferromagnetic enclosures outside the exciting coil ensure protection against stray magnetic fields.

A thorough characterization of the pristine Bi-2212 sample (i.e. without slits) was first performed in axial and transverse configurations in order to determine both the dimensionless shielding factor (SF) of the cylinder, i.e., the ratio of the applied and internal magnetic inductions ($SF = B_{app}/B_{in}$), and its limiting field B_{lim} , i.e., the value of applied magnetic induction above which magnetic shielding degrades and the shielding factor SF drops below a reference level, e.g. $SF < 100$. Experimental data can be found in Ref. [44]. From the results obtained at 77 K, two relevant points should be noticed. First, the limiting field in the transverse configuration B_{lim} is ≈ 18 mT, which corresponds to the best values reported so far for superconducting magnetic shielding at the liquid nitrogen temperature [9, 11, 12-15]. Second, the average critical current density $J_c = 350$ A/cm² corresponds to the self field ~ 20 mT at the surface of the cylinder. As this is comparable to the magnetic field range investigated ($B < 30$ mT), we assumed that both J_c and the critical exponent of the E - J power law $n = 10$ are field independent. These are considered constant in model calculations for the cut sample.

4. Results and discussion

4.1. Distribution of shielding currents

First we investigate the distribution of currents in a short superconducting hollow cylinder containing two axial slits (figure 1 (b)), modelled numerically using the FEM method described in Section 2. The simulations were carried out for several angles θ between the applied magnetic field and the normal to the plane of the slits, as shown in figure 1(b). Figure 2 shows the distribution of the axial component of the current density, J_z , in the median plane of the hollow cylinder for several orientations $0^\circ \leq \theta \leq 90^\circ$ of the transverse field. The amplitude of the applied field is fixed at 30 mT, i.e., above the limiting field B_{lim} of the pristine cylinder. This ensures that the magnetic field penetrated completely through the wall of the cylinder.

For $\theta = 0^\circ$ (i.e. $\mathbf{H} \perp$ slits), the distribution of J_z exhibits an eye-shape structure which is similar to that found in an infinite cylinder without any slit [15, 27]. This is an anticipated result since the shielding

currents in the median plane are always perpendicular to the applied field, i.e. parallel to the slits. Therefore the slits do not affect the current flow in this configuration. Differently stated, two orthogonal symmetry planes appear naturally, one in the direction parallel to the applied field (odd symmetry), and the other one in the perpendicular direction (even symmetry). When the magnetic field is tilted with respect to the normal of the cut, i.e. $\theta > 0^\circ$, the distribution of currents is modified as shown in figure 2(a). The reason is that the screening currents tend to flow along closed loops in planes perpendicular to the applied field, but are interrupted by the slits. It results in a symmetry break and the appearance of a net discontinuity (currents of opposite signs) on both sides of the slit. This configuration can be visualized more clearly in figure 2(b) where the direction of screening currents are schematically illustrated for the particular case of $\theta = 45^\circ$. In this case the shielding currents are forced to follow two separate shielding current loops, and this effect reduces the efficiency of magnetic shielding accordingly (see next section). Finally, the situation where the magnetic field is aligned with the plane of the slits ($\theta = 90^\circ$) allows us to recover two symmetry planes, odd in the direction of the applied magnetic field and even in the perpendicular direction.

4.2. Penetration of magnetic flux density

Figure 3 shows the distribution of magnetic flux density in the hollow cylinder subjected to a 7.5 mT transverse field directed at $\theta = 45^\circ$. Two planes are considered: (a) the median plane ($Z = 0$) and (b) the vertical plane perpendicular to the cut ($X = 0$). The figures demonstrate three penetration routes for the magnetic flux density:

- (i) through the walls of the cylinder, as illustrated by the black arrows in figures 3(a) and 3(b);
- (ii) through the open ends at the top and bottom of the cylinder, as illustrated by the grey arrows in figure 3(b);
- (iii) through two slits, as illustrated by the white arrows in figure 3(a).

As can be seen in figure 3(a), the magnetic flux density at the centre of the cylinder (B_{in}) is clearly deflected with respect to the applied flux density (B_{app}). This misalignment can be considered as a result of “competition” between symmetry, which tends to be imposed by the applied field, and the presence of the cut, which allows direct magnetic flux penetration. In order to quantify the relative contribution of magnetic flux density entering through the cut, we define φ as the angle between B_{in} at the centre of the cylinder and the external magnetic field B_{app} . The variation of φ with respect to the angle and amplitude of the applied field will be studied in the next section.

4.3. Angle between the applied field and the internal field

We now investigate how the angle φ between internal and applied field varies as a function of angle θ between the applied field and the normal of the cut. The results of modelling are shown in figure 4(a) for three amplitudes of the applied field. The φ vs θ curves are found to exhibit a pronounced maximum, which can be better understood using schematic illustrations shown in figure 4(b). For $\theta = 0^\circ$, the applied field is perpendicular to the cut which therefore has no influence on the shielding currents ($\varphi = 0^\circ$). For $\theta = 90^\circ$, the applied field is directed along the cut plane which offers a preferential channel for flux penetration; by symmetry the internal field B_{in} is thus aligned with the applied field B_{app} and one has again $\varphi = 0^\circ$. In the intermediate situation ($0^\circ < \theta < 90^\circ$), the competing mechanisms discussed above lead to a misalignment between B_{in} and B_{app} , yielding a finite value of φ and a φ vs θ curve displaying a maximum, as shown in figure 4(a). Interestingly, the modelling predicts non symmetrical curves, with the maximum deflection occurring for θ between 50° and 55° in the magnetic field range investigated. Figure 4(c) shows the experimental data measured on a Bi-2212 cylinder having the same dimensions as that used for modelling. As can be seen, the measured curves largely agree with the modelled ones. Small differences are observed. First, a deflection of $\varphi \approx 2.5^\circ$ is measured when the field is either normal or parallel to the cut. This can be attributed to the small signal-to-noise ratio of the perpendicular component (theoretically zero) of the measured magnetic induction for these angles and will not be discussed further. Second, the experimental curves are somewhat flattened compared to the modelled curves: the maximum value of φ at 7.5 mT is 29° for the modelling against 21° for the experiment. This is likely due to the finite active area of the Hall sensor ($100 \mu\text{m} \times 100 \mu\text{m}$), which results in a smearing of the measured flux density, and from the differences in modelled and actual gap sizes, which may affect the relative importance of a penetration occurring through the slits. Apart from these minor differences, the overall agreement is very good. It should be recalled here that the modelling was carried out without adjustment of free parameters: the J_c and n values (both supposed field-independent) being taken directly from experimental data measured on the pristine sample.

It is of interest to investigate how the amplitude of the applied magnetic field affects the value of φ . The φ vs B_{app} curve modelled for the applied field directed at $\theta = 45^\circ$ is plotted on figure 5(a). As can be seen, the modelling predicts a maximum value of φ , albeit relatively flat. This indicates that the magnetic flux channelling through the two slits dominates in some range of applied fields. This can be interpreted as follows. At low applied field B_{app} , the internal field B_{in} is very small, but the main contribution arises from flux entering from the top and bottom of the cylinder, through large open ends. The relative orientation of the cut and the applied field does not affect much the internal field,

and hence the misalignment φ is small. For large applied fields B_{app} , the magnetic flux enters mainly through the walls of the superconductor, as is the case for a sample without cut, and the angle φ is expected to approach 0 at high fields. In between, the angle φ exhibits a well-defined maximum, as shown in figure 5(a). The corresponding experimental data are plotted in figure 5(b). Due to the signal averaging over the active area of the Hall probe, the measured values of φ are found to be smaller than those obtained by simulation, as is the case in figure 4. Remarkably however, the maximum predicted by modelling can be clearly seen in the experiment.

4.4. Magnetic shielding curves

In this last section, we study the magnetic shielding curves of the cut cylinder, i.e. the magnetic flux density in the centre of cylinder B_{in} as a function of the applied field B_{app} . Because of the angle between B_{in} and B_{app} , we focus here on the component of B_{in} parallel to the applied field, hereafter noted “ $B_{||}$ ”. The modelled results are shown in figure 6(a) for various orientations $0^\circ \leq \theta \leq 90^\circ$ of the transverse field. Figures 6(b) and 6(c) show the corresponding experimental data measured on a bulk Bi-2212 sample with the same geometry as the modelled structure (figure 6(b)), or the same radius but four times the height of the modelled structure (figure 6(c)).

We first discuss the modelled data (figure 6(a)). When $\theta = 90^\circ$ (magnetic field parallel to the slits) the magnetic shielding is very weak, i.e. $B_{||} \sim 0.6 B_{app}$. On lowering θ , a more pronounced shielding effect appears, yielding for the best orientation ($\theta = 0^\circ$) $B_{||} \sim 0.28 B_{app}$ at 10 mT. Although the presence of the slits has no effect on the magnetic flux penetration at this particular angle, the magnetic shielding is relatively poor because the magnetic field penetrates the short cylinder from the top and the bottom.

As can be seen from figure 6(b), the experimental results obtained with the same geometry remarkably agree with the modelling. For $\theta = 0^\circ$, $B_{||} \sim 0.27 B_{app}$ at 10 mT. This excellent agreement makes us confident in the fact that all penetration routes for the magnetic field are properly taken into account by our modelling tool.

The shielding performances can be improved significantly by increasing the aspect ratio of the structure. Figure 6(c) show the B_{in} vs B_{app} curves measured on a sample with larger aspect ratio (length 80 mm, average diameter 21 mm), which is more representative of a practical case. With such dimensions, notable shielding ($B_{in} < 0.01 B_{app}$) is observed for $B_{app} < 18$ mT and $\theta = 0^\circ$. For increasing θ , magnetic shielding degrades, as is the case for the short sample. This feature appears more clearly in figure 7, showing the shielding factor (SF) as a function of the applied magnetic field. The shielding

factor SF is defined here as B_{app}/B_{in} , where B_{in} denotes the component ($B_{||}$) parallel to the applied field B_{app} . Experimentally, the shielding factor is found to exhibit remarkably high values ($SF > 100$) for $\theta \leq 15^\circ$ but the magnetic shielding efficiency deteriorates when the angle between the applied transverse magnetic field and the normal to the slit plane exceeds 15° .

From the data displayed in figures 5 and 6, it is worth noting that the modelling is able to reproduce experimental data although Meissner currents are totally neglected. There are likely two reasons for this. The first is that the superconductor is modelled by a E - J power law and not through a critical state analysis (Bean model); the latter would possibly require amending the model by considering that vortices do not penetrate below the lower critical field H_{c1} . In the present case, the only constitutive law (and hence, superconducting parameters) involve J_c and n . Since these parameters are considered to be field-independent, it seems that the value of H_{c1} compared to H_{app} can be neglected as well. Second, the data are measured at liquid nitrogen temperature (77 K), i.e. close to T_c (~ 90 K). Hence the lower critical field is quite small and flux creep effects due to thermally activated vortex motion are found to play a major role. As a consequence, the threshold field of the pristine structure is found to depend on the sweep rate of the applied magnetic field (which would not be the case for Meissner currents). This feature is reflected by the relatively small n value ($n \sim 10$) used in our modelling.

5. Conclusions

We have investigated the magnetic flux penetration in a bulk hollow superconducting cylinder of finite height containing two axial slits. The cylinder was subjected to a transverse field directed at several angles with respect to the cut plane. This study was performed both numerically and experimentally.

The Finite Element Method (FEM) model, based on the open-source solver GetDP, was used with a three-dimensional (3D) geometry in order to account for non-symmetrical arrangements of the magnetic field and the superconductor. The results show how the slits block the shielding currents loops and act as an “entrance channel” for the magnetic flux. Three penetration routes of the magnetic flux are identified: (i) the walls of the cylinder, (ii) the opening ends at the top and bottom and (iii) the two slits. The finite contribution of the flux entering through the slits to the total flux density in the cylinder gives rise to a misalignment between the applied field B_{app} and the internal field B_{in} . The angle φ between the two fields is found to be a non-monotonic function of both the applied field direction θ and amplitude B_{app} .

The modelled flux penetration was compared with the experimental results on bulk Bi-2212 cylinder measured with a high-sensitivity Hall probe. Although the modelled angle φ is found to be overestimated with respect to experimental data, the overall agreement is very good and the qualitative features observed in the experiment can be reproduced by the model. In particular, the field amplitude dependence of the angle φ exhibits a relatively flat profile with a well-defined maximum, representative of the competition between the penetration routes for the magnetic flux as the applied field changes.

In this study we intentionally minimised the set of parameters used in the model, since the use of additional material-dependent data increases uncertainty and complicates significantly the understanding of their influence on the final results. The results obtained in the present work are based on a critical current density J_c and a power law exponent n , assumed to be field-independent and determined from independent preliminary measurements on the superconducting cylinder before cutting. The data show clearly that the principal features can be reproduced without sophisticated constitutive laws. The excellent agreement between simulation and experiment also validates the used simulation tools. These will be a valuable help for the design of larger shielding devices, especially with respect to an optimized choice of geometry and position of the interfaces, if more than one bulk part is to be used. It is worth emphasizing that the model can be combined with more complex parameters, including e.g. field-dependent superconducting properties, or any time-dependent waveform of the applied magnetic field.

Acknowledgments

We thank the FRS-FNRS, the *Communauté Française de Belgique* for cryofluid, travel and equipment grants, under references CR.CH.09-10-1.5.212.10 and ARC 11/16-03. Fruitful and enlightening discussions with M O Rikel (Nexans Superconductors) are also greatly acknowledged.

References

- [1] Pavese F 1998 *Handbook of Applied Superconductivity* (IoP Publishing) 1461
- [2] Fagnard JF, Vanderheyden B and Vanderbemden P 2012 *Superconductivity: Recent Developments and New Production Technologies* (Nova Science Publishing), in press
- [3] Willis J O, McHenry M E, Maley M P and Sheinberg H 1989 *IEEE Trans. Magn.* **25** 2502
- [4] Kamiya K, Warner B and DiPirro M 2001 *Cryogenics* **41** 401
- [5] Pizzella V, Della Penna S, Del Gratta C and Luca Romani G 2001 *Supercond. Sci. Technol.* **14**

R79

- [6] Giunchi G, Bassani E, Cavallin T, Bancone N and Pavese F 2007 *Supercond. Sci. Technol.* **20** L39
- [7] Holmes J. J 2008 *Synthesis Lectures on Computational Electromagnetics* **3** 1
- [8] Rabbers J J, Oomen M P, Bassani E, Ripamonti G and Giunchi G 2010 *Supercond. Sci. Technol.* **23** 125003
- [9] Fagnard J-F, Elschner S, Bock J, Dirickx M, Vanderheyden B and Vanderbemden P 2010 *Supercond. Sci. Technol.* **23** 095012
- [10] Gozzelino L, Minetti B, Gerbaldo R, Ghigo G, Laviano F, Lopardo G, Plapcianu C, Agostino A, Cagliero S, Truccato M, Zilberti L and Mezzetti E 2011 *J. Supercond. Nov. Magn.* **24** 307
- [11] Fagnard J-F, Dirickx M, Levin G A, Barnes P N, Vanderheyden B and Vanderbemden P 2010 *J. Appl. Phys.* **108** 013910
- [12] Matsuba H, Yahara A and Irisawa D 1992 *Supercond. Sci. Technol.* **5** S432
- [13] Plechacek V, Hejtmanek J, Sedmidubsky D, Knizek K, Pollert E, Janu Z and Tichy R 1995 *IEEE Trans. Appl. Supercond.* **5** 528
- [14] Denis S, Dusoulier L, Dirickx M, Vanderbemden P, Cloots R, Ausloos M and Vanderheyden B 2007 *Supercond. Sci. Technol.* **20** 192
- [15] Fagnard J-F, Dirickx M, Ausloos M, Lousberg G, Vanderheyden B and Vanderbemden P. 2009 *Supercond. Sci. Technol.* **22** 105002
- [16] Bock J, Elschner S and Herrmann P 1995 *IEEE Trans. Appl. Supercond.* **5** 1409
- [17] Elschner S, Bock J Brommer G, Cowey L 1999 *Appl. Supercond.* **167** 1029
- [18] Elschner S, Bock J 1992 *Adv. Mat.* **4** 242
- [19] Frankel D 1979 *IEEE Trans. Magn.* **MAG-15** 1349
- [20] Plechacek V, Hejtmanek J, Sedmidubsky D, Knizek K, Pollert E, Janu Z and Tichy R 1995 *IEEE Trans. Appl. Supercond.* **5** 528
- [21] Bhagwat K V and Chaddah P 1991 *Phys. Rev. B* **44** 6950
- [22] Bean C 1962 *Phys. Rev. Lett.* **8** 250
- [23] Campbell A 1991 *IEEE Trans. Magn.* **27** 1660
- [24] Fagnard J-F, Denis S, Lousberg G, Dirickx M, Ausloos M, Vanderheyden B and Vanderbemden P 2009 *IEEE Trans. Appl. Supercond.* **19** 2905
- [25] Navau C, Sanchez A, Pardo E, Chen D-X, Bartolomé E, Granados X, Puig T and Obradors X 2005 *Phys. Rev. B* **71** 214507
- [26] Denis S, Dirickx M, Vanderbemden P, Ausloos M and Vanderheyden B 2007 *Supercond. Sci. Technol.* **20** 418
- [27] Carr W. J 2001 *AC Loss and Macroscopic Theory of Superconductors* (CRC Press) 212
- [28] Zolotovskii A B, Reiderman A F, Glazer B. A, Lappo I. S, Lyakin V V and Raevskii V Y 1991 *Superconductivity* **4** 810

- [29] Zhilichev Y N 2000 *IEEE Trans. Appl. Supercond.* **10** 1657
- [30] Mawatari Y 2011 *Phys. Rev. B* **83** 134512
- [31] Brandt E H 1998 *Phys. Rev. B* **58** 6506
- [32] Brandt E H 1996 *Phys. Rev. B* **54** 4246
- [33] Hong Z, Campbell A M and Coombs T. A 2006 *Supercond. Sci. Technol.* **19** 1246
- [34] Lousberg G. P, Ausloos M, Geuzaine C, Dular P, Vanderbemden P and Vanderheyden B 2009 *Supercond. Sci. Technol.* **22** 055005
- [35] Grilli F, Stavrev S, Le Floch Y, Costa Bouzo M, Vinot E, Klutsch I, Meunier G, Tixador P and Dutoit B 2004 *IEEE Trans. Appl. Supercond.* **15** 17
- [36] Wolsky A M and Campbell A M 2008 *Supercond. Sci. Technol.* **21** 075021
- [37] Zhang M and Coombs T A 2012 *Supercond. Sci. Technol.* **25** 015009
- [38] Henrotte F, Meys B, Hedia H, Dular P and Legros W 1999 *IEEE Trans. Magn.* **35** 1434
- [39] <http://ace.montefiore.ulg.ac.be>
- [40] <http://geuz.org/getdp>
- [41] Brandt E H and Mikitik G P 2007 *Phys. Rev. B* **76** 064526
- [42] Clem J R, Weigand M, Durrell J H and Campbell AM 2011 *Supercond. Sci. Technol.* **24** 062002
- [43] Ruiz H S, Badia-Majos A and Lopez C 2011 *Supercond. Sci. Technol.* **24** 115005
- [44] Fagnard J-F 2011 Experimental and numerical study of the factors influencing the performances of magnetic screens made of high temperature superconductors *PhD Thesis* University of Liège

Table 1. Geometrical characteristics of the Bi-2212 hollow cylinder.

Material	$\text{Bi}_2\text{Sr}_2\text{CaCu}_2\text{O}_8$
Length	$\ell = 80$ mm (long sample) $\ell = 20$ mm (short sample)
Inner radius	$a_1 = 8$ mm
Wall thickness	$e = 5$ mm
Gap width of the slit	$w \approx 200$ μm

Figure 1

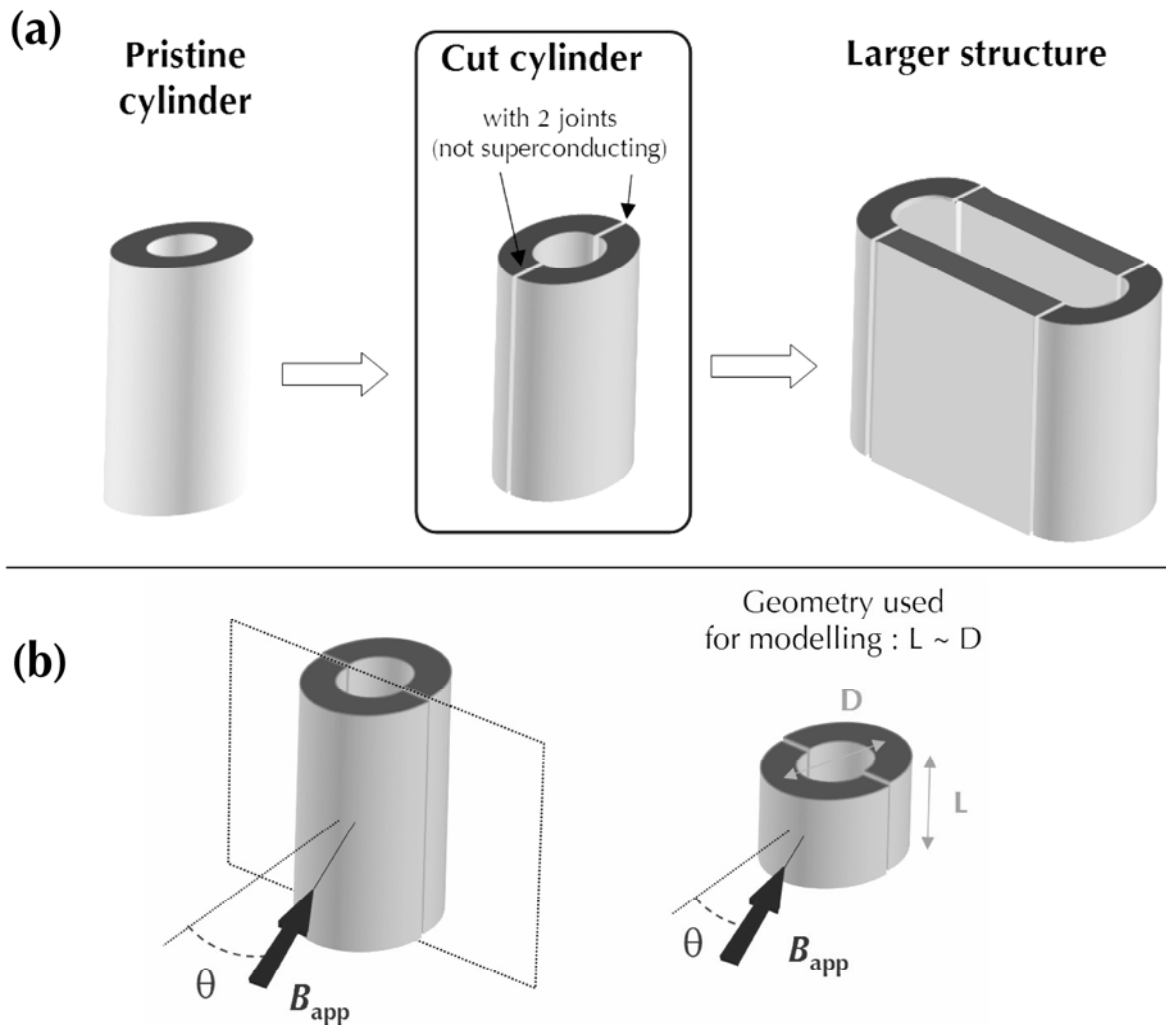


Figure 1. (a) Schematic illustration of a hollow cylinder (Pristine cylinder), a hollow cylinder cut axially (Cut cylinder) and a structure made of two half-cylinders joined by two rectangular plates (Larger structure). (b) Schematic illustration of a cut hollow cylinder having (left) a large aspect ratio and (right) an aspect ratio close to unity. The experiments are carried out on the cylinders with both large and small aspect ratios, while modelling is carried out on the short cylinder only. The transverse magnetic field B_{app} is applied with an angle θ with respect to the normal to the plane of the cut.

Figure 2

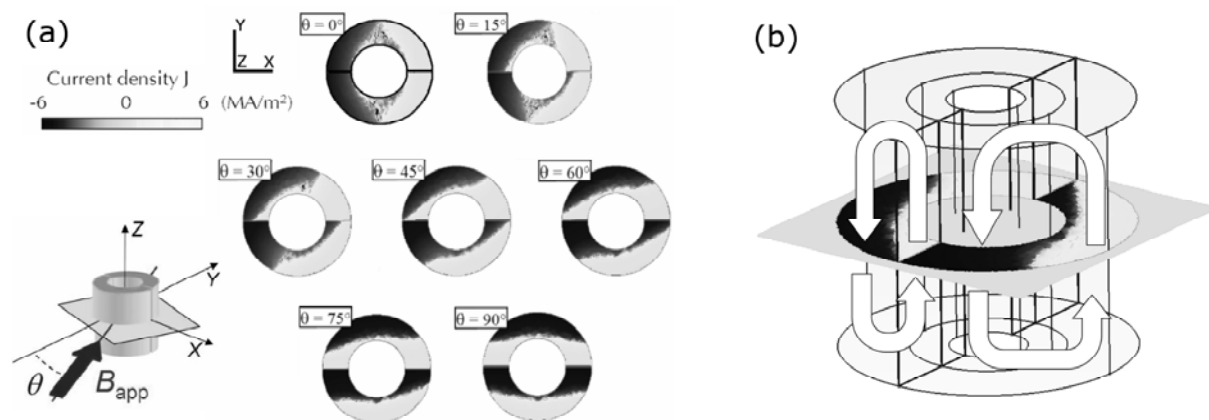


Figure 2. (a) Modelled distribution of J_z in the plane $Z = 0$ of a cut hollow cylinder subjected to a transverse magnetic field $\mu_0 H_{\text{app}} = 30$ mT directed at several angles θ with respect to the normal to the plane of the cut. (b) Schematic illustration of the direction of screening currents in the particular case $\theta = 45^\circ$.

Figure 3

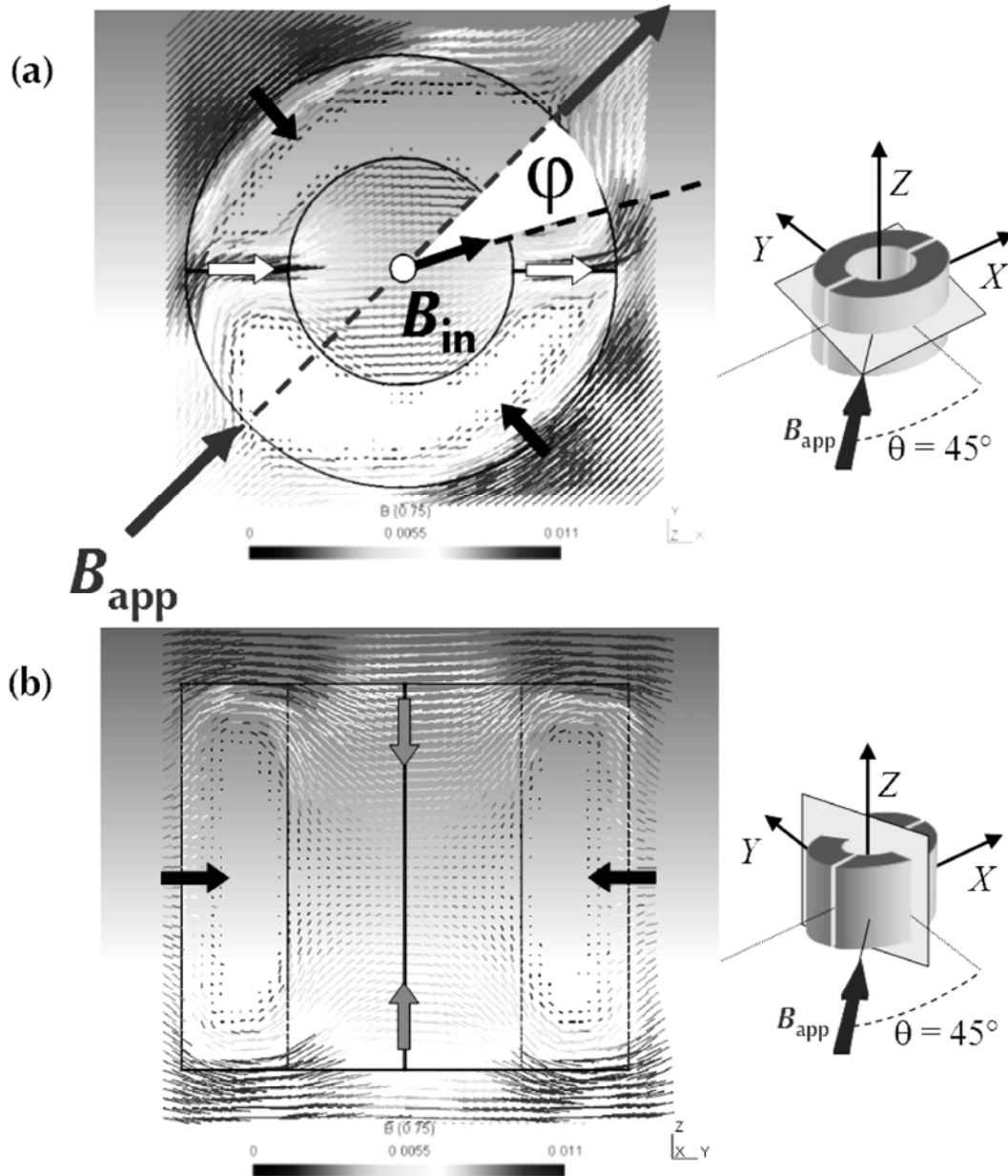


Figure 3. Modelled distribution of magnetic flux density lines B for a transverse magnetic field $B_{app} = \mu_0 H_{app} = 7.5$ mT applied at an angle $\theta = 45^\circ$ with respect to the normal of the plane containing the two slits ($Y = 0$). The two pictures show the distribution of B (a) in the plane $Z = 0$ and (b) in the plane $X = 0$. The angle ϕ is defined as the angle between the applied induction B_{app} and the magnetic induction at the centre of the cylinder B_{in} .

Figure 4

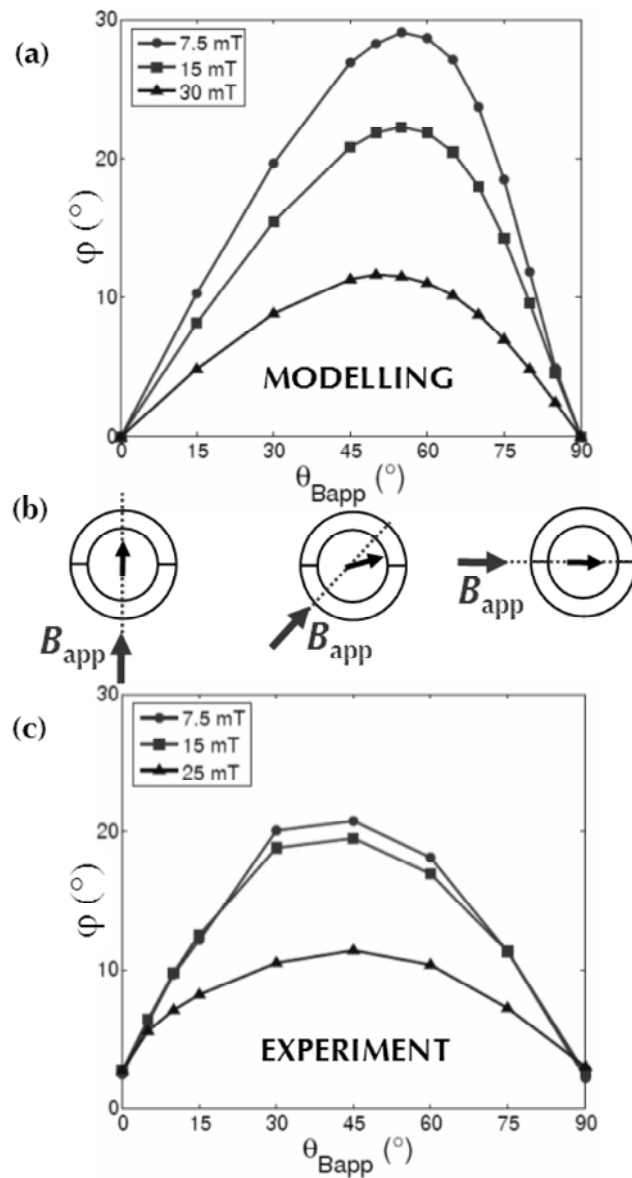


Figure 4. (a) Modelled angular difference ϕ (between the applied field $\mu_0 H_{app}$ and the magnetic induction at the centre of the cylinder B_{in}) as a function of the angular position θ of the applied field for several amplitudes equal to (circles) $\mu_0 H_{app} = 7.5$ mT, (squares) $\mu_0 H_{app} = 15$ mT and (triangles) $\mu_0 H_{app} = 30$ mT. (b) Schematic illustration of the configurations corresponding to $\theta = 0^\circ$, $\theta = 45^\circ$ and $\theta = 90^\circ$. (c) Experimental data measured on a bulk Bi-2212 structure having nearly the same dimensions: measured angular difference ϕ as a function of the angular position θ of the applied field for several amplitudes equal to (circles) $\mu_0 H_{app} = 7.5$ mT, (squares) $\mu_0 H_{app} = 15$ mT and (triangles) $\mu_0 H_{app} = 25$ mT.

Figure 5

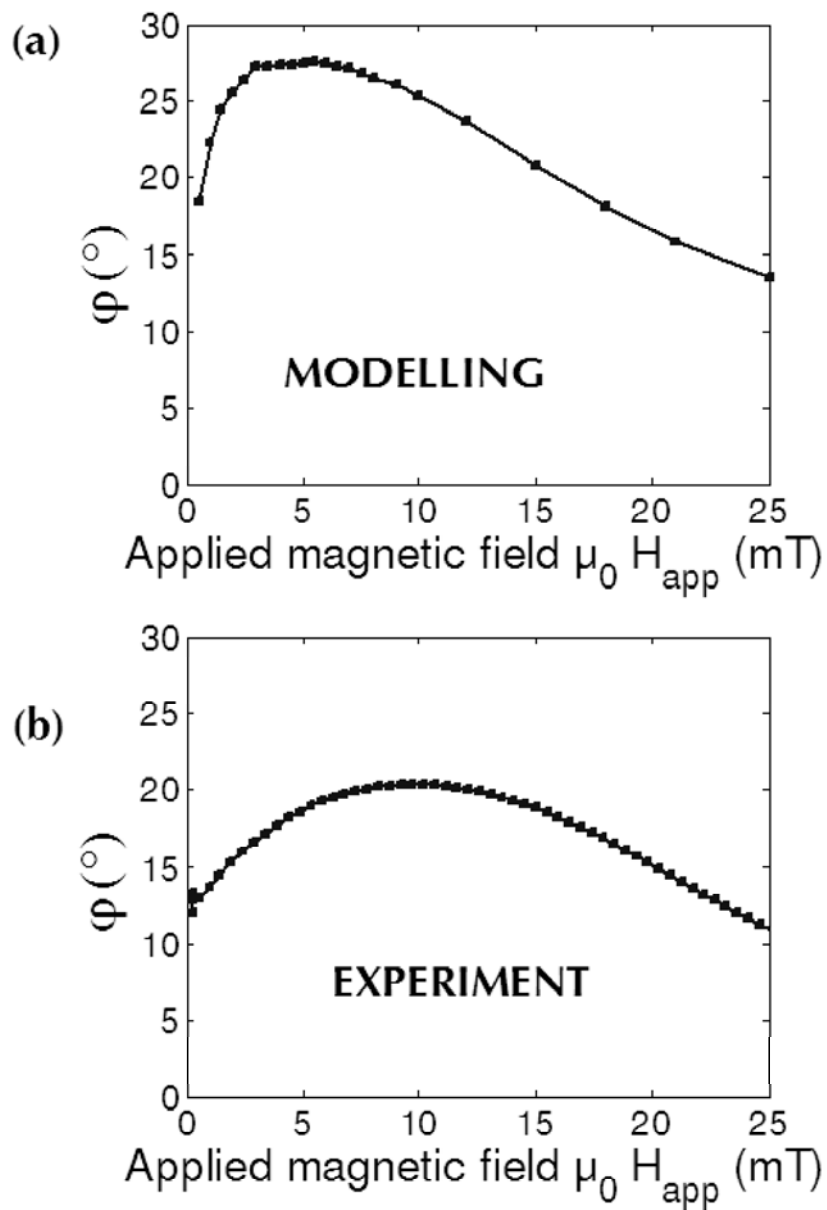


Figure 5. (a) Modelled angular difference ϕ (between the applied field $\mu_0 H_{app}$ and the magnetic induction at the centre of the cylinder B_{in}) as a function of the amplitude of the transverse magnetic field applied at angle $\theta = 45^\circ$. (b) Experimental data measured on a bulk Bi-2212 structure having nearly the same dimensions: measured angular difference ϕ as a function of the amplitude of the transverse magnetic field applied at angle $\theta = 45^\circ$.

Figure 6

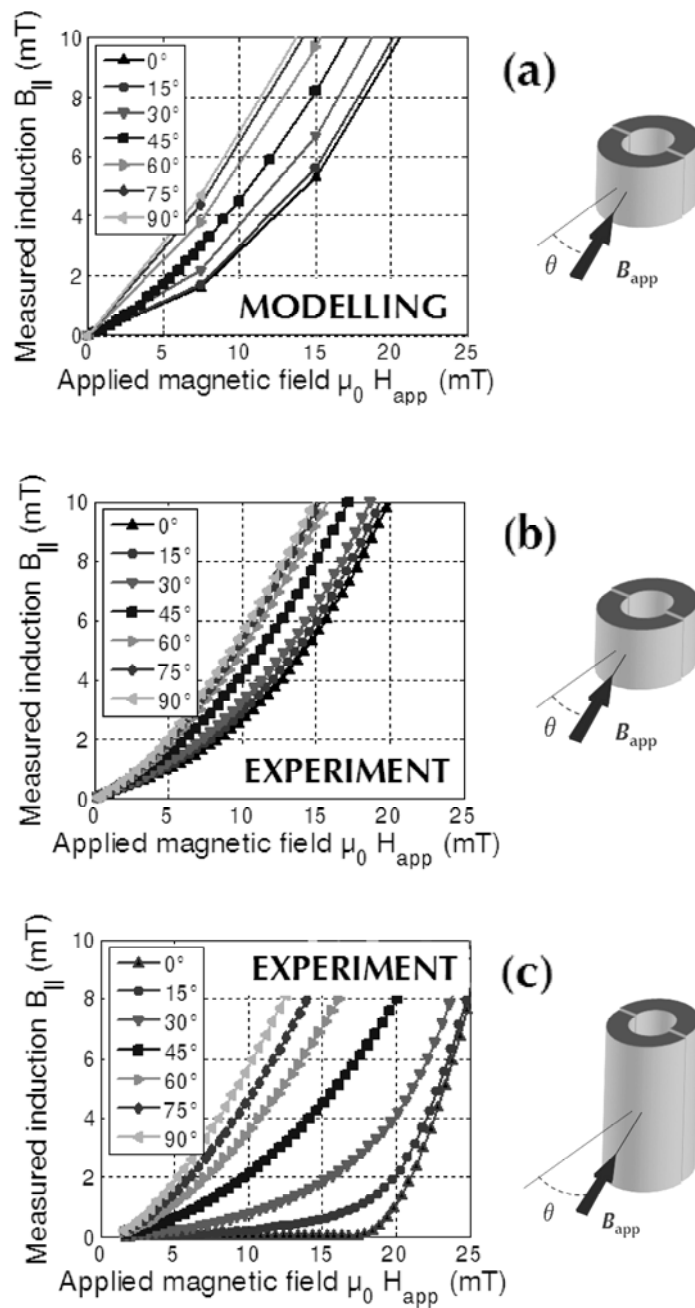


Figure 6. Magnetic induction B_{in} at the centre of a hollow superconducting cylinder containing two slits as a function of the applied magnetic field B_{app} . The applied field is directed at several angles θ with respect to the normal to the plane containing the two slits and the graphs show the B_{in} component ($B_{||}$) parallel to the applied field B_{app} . (a) Modelled data for a cylinder having an aspect ratio close to unity. (b) Data measured on a bulk Bi-2212 cylinder of nearly the same dimensions. (c) Data measured on a bulk Bi-2212 cylinder whose radius is the same and height is four times that of (a) and (b).

Figure 7

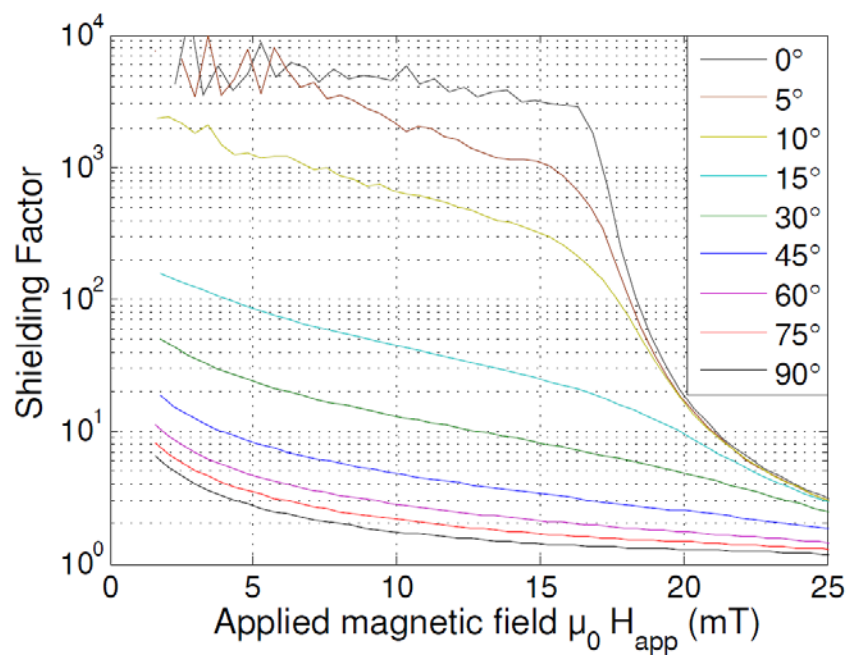


Figure 7. Shielding factor at the centre of the long hollow superconducting cylinder (length 80 mm) containing two slits as a function of the applied magnetic field B_{app} . The applied field is directed at several angles θ with respect to the normal to the plane containing the two slits. The curves from top to bottom refer to increasing values of θ .